Optical properties of two-dimensional and three-dimensional inhomogeneous media: a renormalization approach

1990 J. Phys.: Condens. Matter 2 8651

(http://iopscience.iop.org/0953-8984/2/43/010)

J. Phys.: Condens. Matter **2** (1990) 8651–8668. Printed in the UK

Optical properties of two-dimensional and three-dimensional inhomogeneous media: a renormalization approach

K Driss-Khodja†‡ and S Berthier‡

† Laboratoire d'Optique des Solides, Unité associée au CNRS D 0781, Université Pierre et Marie Curie, 4 place Jussieu, 75252 Paris Cédex 05, France

‡ Unité de Recherche en Physique du Solide, Université d'Oran-es-Sénia, Algeria

Received 19 February 1990, in final form 8 June 1990

Abstract. We propose a position space renormalization group approach based on the Kadanoff block method, for the calculation of an effective dielectric function of cermet-type films (3D) or island films (2D). These models have been applied to simulated lattices and to digitized transmission electron micrographs of 2D and 3D systems. The results account for both the resonant absorption and the optical crossover corresponding to the metal-to-non-metal transition. The effective dielectric function is in very good quantitative agreement with most of the experimental data, even near the percolation threshold where it is found to obey scaling laws with critical exponents very close to the theoretical values.

1. Introduction

The determination of the dielectric function of inhomogeneous media (cermet films or thin island films) is a very old unsolved problem, which is still of great interest. The history of the research on optical properties of inhomogeneous materials dates back to the beginning of the nineteenth century with the important work of Maxwell Garnett (MG) (1904, 1906) and Mie (1908). (For a historical overview of the various effective-medium theories, see Niklasson's (1982) thesis.) The most important progress since these pioneering studies has been the introduction of the mean-field concept in the effective-medium theories of Bruggeman (1935); both the metal-to-non-metal transition (Berthier *et al* 1987a, b) and the so-called dielectric anomaly or resonant absorption, characteristic of the metallic granular compounds, are qualitatively modelled. All these theories, as well as many others (e.g. those of Ping Sheng (1980) and Cohen *et al* (1973)), are 3D theories. The first attempt to model a 2D system seems to be also attributed to Bruggeman who introduced an effective parameter connected with the dimensionality of the system. However, the environment of the film (the substrate–film and film–air interfaces) is neglected and this approach cannot be considered as a 2D theory. The interaction between the dipole particle and its mirror image and with all the dipole–dipole image couples was first introduced by Yamaguchi *et al* (1973, 1974) and Yoshida *et al* (1971). At the same time, Bedeaux and Vlieger (1973, 1974, 1983) took into account the effect of the substrate by using surface dielectric coefficients. The above approaches require the filling factor to be small and cannot be used for phase transition modelling.

0953-8984/90/438651 + 18 $03.50

In these 2D and 3D theories, the morphology of the medium is taken into account roughly via the introduction of a unit cell describing schematically the relative situation of the constituents, their respective shape and volume fraction (Ping Sheng 1980, Berthier and Lafait 1986). However, it has been observed in many systems that the shape, size and orientation of the inclusions are highly correlated and depend on the concentration. It is clear that the morphology of the clusters, which is branched and often fractal around the electrical percolation (Laibowitz *et al* 1982), is the main parameter of the problem and can never be reduced to a simple unit cell.

To take into account the real structure of the inhomogeneous medium, we have proposed a 2D and 3D effective-medium theory based on a position space renormalization procedure (Berthier *et al* 1987b, Berthier and Driss-Khodja 1989). These models use the Kadanoff (1966) block technique (see also Kadanoff *et al* 1967) and were applied to randomly occupied square lattices generated by a computer. In this paper, we attempt to apply this procedure to real digitized transmission electron micrographs of 2D and 3D systems and to compare the results with the predictions of the other theories as well as with experimental results.

In section 2, we briefly present the experimental techniques of deposition and characterization of the 2D and 3D films, with particular attention to the image treatment since this information is of great importance for the development of the renormalization process. Section 3 is devoted to a detailed description of the Kadanoff block method applied to the effective dielectric function calculation. This is independent of the dimensionality of the system. In sections 4 and 5 we present the applications of the above principle to 3D and 2D media, respectively. The well known MG formulation which appears in the calculation of the 3D effective dielectric function is briefly outlined together with its limitations. On the contrary, the recent and less currently used 2D approach of Yoshida *et al* and Yamaguchi *et al* and the modifications introduced for its application in the renormalization process is described at length. In both cases, we recall the main results obtained on computed simulated lattices (theoretical critical exponents for effective polarization and effective conduction). The process is then applied to real 3D ($Pt–Al_2O_3$) and 2D (Au island films) systems and the effective calculated dielectric function is compared with experimental results as well as with other theoretical predictions (the theory of Yoshida *et al* and Yamaguchi *et al* for 2D systems, and the MG and Bruggeman theories for 3D systems).

2. Preparation and characterization of inhomogeneous films

2.1. Preparation and characterization

$Pt–Al_2O_3$ films (Berthier and Lafait 1982) were deposited onto optically polished glass by RF cosputtering. The target is composed of an Al_2O_3 disc with circular holes filled with platinum pellets. The composition of the film can be varied over a wide range according to the number of platinum pellets in use. The substrates are located on a rotating sample holder in order to homogenize the composition of the deposit and the film thickness.

Thin gold granular films were deposited onto glass substrates at room temperature by thermal evaporation under an ultrahigh vacuum (Gadenne 1987).

The thicknesses of the films were determined by x-ray interference under grazing incidence and the composition of the cermet deposit (metallic volume fraction q) was

determined by electron microprobe analysis. For granular films, the metal volume fraction q is extracted by an appropriate image treatment as described in section 2.4.

2.2. Experimental determination of the percolation threshold

The electrical percolation threshold of cermet films can be estimated from DC resistance measurements. We obtained $q_c = 0.43 \pm 0.02$ for the Pt–Al_2O_3 films series. In a previous paper (Berthier *et al* 1987a) we presented a determination of the critical concentration based on optical measurements.

The value of q_c obtained with this method for Pt–Al_2O_3 thin films is 0.40 ± 0.02. To within the resolution of the data, these two techniques are in relatively good agreement and do not allow one to distinguish the electrical from the optical percolation threshold. The effective resistivity of the Au granular films was deduced from the DC electrical resistance $r_\square$ and the deposited mass corresponding to a mass thickness d_m (Gadenne *et al* 1988). Gadenne *et al* also presented an optical determination of the percolation threshold from optical absorption measurements, as described for the transmissivity of granular films by Yagil and Deutscher (1987). Following these observations the critical concentration q_c of Au island films is about 0.61 ± 0.01.

2.3. Image treatment

Considering the predominant role of the morphology of the films in their transport and optical properties, the image treatment is an essential step in our real-space renormalization process; in addition, for any further statistical treatments and characterizations (concentration, cluster morphology, etc), exact knowledge of the morphology of the media is necessary. Beghdadi *et al* (1984) have developed optimum image processing for the morphological study of granular films. They presented the different steps from the transmission electron micrographs of the thin films up to a binary image of the digitized films. The sequence is as follows:

(i) digitization of the micrograph;
(ii) correction of non-homogeneous illumination effects;
(iii) binarization and contrast enhancement.

These steps will not be developed here but we paid much attention to the quality criteria used at each step of the process. As will be seen later, no free parameter is introduced into the renormalized effective-function model. Nevertheless, a fitting procedure of the volume fraction can be attempted by modifying the threshold in the binarization process, and the apparent volume fraction on the image can be varied over a few per cent.

3. The renormalization process

The principle of the method is the same as that introduced for spins in magnetic materials by Kadanoff (1966) (see also Wilson 1974); in a region small compared with the correlation length, the spins are grouped into blocks of n spins each, every spin having only two possible states (up or down). From a wider point of view, the group behaves like a single effective spin and the original lattice can be replaced by a larger lattice. The effective lattice is then renormalized to conserve the spin magnitude. At the end of the

process, a macroscopic point of view is reached and macroscopic effective quantities can be determined. Following Kadanoff's idea, Bernasconi (1978) proposed a real-space renormalization approach to the conductivity of a bond-disordered conductance lattice. We present here a similar process for the dielectric function of an inhomogeneous medium.

Let us start from a binarized transmission electron micrograph of a thin film. This micrograph is in fact the initial square lattice of the process (size ξ; generally $\xi = 512$), each pixel of the lattice having two possible states: black or white, i.e. metallic or dielectric. The pixels are then characterized by the respective dielectric functions of the components; generally ε_d = constant for the dielectric. The dielectric function of the metal is either determined on thin films of pure metal prepared in the same deposition conditions as the inhomogeneous sample or characterized by the Drude expression using theoretical considerations: $\varepsilon_m(\omega) = P - \omega_p^2/\omega(\omega + i/\tau)$. The initial lattice is divided into blocks of four pixels each. Each block is then considered as a super-pixel whose effective dielectric function has to be determined using an effective-dielectric-function theory which depends on the dimensionality of the system. These theories will be detailed in the next section but it should be noted, at this point, that most of the theories could equally apply to more than two components. Nevertheless, from practical considerations, we limit the components to two. It is then obvious that in most cases the new super-blocks obtained after the first step are composed of four different constituents. Continuing with the effective-medium theories and unit-cell concepts implies new simplifying assumptions. The four components of any block at step n are reduced to two by an averaging process applied on the one hand to the metallic-like components and on the other hand to the dielectric-like components, according to

$$\bar{\varepsilon}_n = \sum_j q_j \varepsilon_n^j \tag{1}$$

where j denotes the different components of each dielectric or metallic class; this averaging process is valid as long as the dielectric functions of both classes are not very different (Landau *et al* 1969). At any step, we then have two components: a dielectric component and a metallic component. Later, whatever the effective-medium theory used, it is necessary to decide for each block which component is the matrix and which is the inclusion. We retain the following conduction criterion: the matrix in the unit cell (dielectric function ε^{ma}) is the average component through which one can go from one side of the block to the other, following the field direction. For two sites connected by one corner, two different cases are to be considered (conducting or non-conducting convention). Each block can then be reduced to a unit cell with spherical or ellipsoidal inclusions (dielectric function ε^i). To this end, a simple likeness criterion is used (figure 1); a single site is schematized by a sphere with volume fraction $q = \frac{1}{4}$, and two adjacent sites are schematized by a prolate ellipsoid, either parallel or perpendicular to the electric field, with a volume fraction $q = \frac{1}{2}$ and an axis ratio $c/a = 2$. In the parallel case, a size effect can be introduced by modifying the effective relaxation time τ entering the Drude expression above, with r enhanced by a factor of 2. For two sites connected by one corner, the criterion is more arbitrary. It has been schematized by a sphere with volume fraction $q = \frac{1}{2}$. A more realistic model could be envisaged: a prolate ellipsoidal particle ($c/a = 2$) at an angle of 45° to the field direction. The shape and orientation of the particle are introduced into the theories via the depolarization factor L_i. In the direction of the electric field, L_i is related to the axis ratio c/a of the prolate ellipsoidal particle via the equation $L_\parallel = \{[\ln(1+e)]/(1-e) - 2e\}(1-e^2)/2e^3$, $L_\perp^i = (1 - L_\parallel)/2$ with

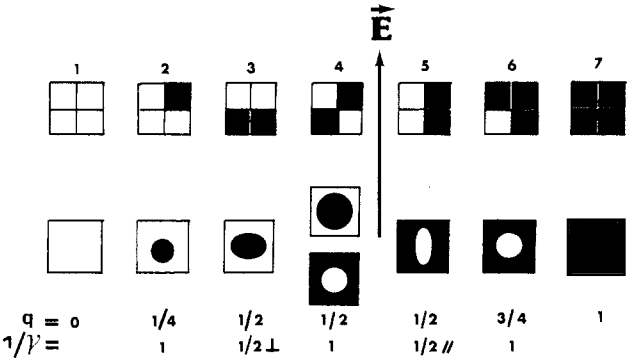

Figure 1. The different block configurations and the corresponding unit cells (dielectric is in white, and metal in black). In case 4, two cells can be defined, whether the diagonal is conducting or not. In this and the following figures the conducting and non-conducting conventions will be indicated by a large full square and a large open square, respectively.

$e = (1 - a^2/c^2)^{1/2}$ (Lamb *et al* 1980) ($L_i = \frac{1}{3}$ for a spherical inclusion). For $c/a = 2$, $L_{\parallel} = 0.2364$ if the field is parallel to the main axis, and $L_{\perp} = 0.3818$ in the perpendicular case. For non-parallel inclusions, the depolarization factor is a tensor with an eigenvalue in the field direction given by $L^{\alpha} = L_{\parallel}L_{\perp}/(L_{\parallel}\cos^2\alpha + L_{\perp}\sin^2\alpha)$ (Berthier 1988); for $c/a = 2$ and $\alpha = 45°$, $L^{\alpha} \simeq 0.3045$.

We shall now apply this general principle to the 2D and 3D effective dielectric functions. In a first approach, a computer-simulated lattice 2D randomly occupied square is used for general considerations. Then the model is applied to digitized transmission electron micrographs for comparison with experimental results.

4. Three-dimensional model

The local effective dielectric function of each block at any step n has to be determined by the use of a theory which neglects interactions with the surrounding blocks; these interactions are taken into account in an implicit way by the renormalization process. The MG theory, as modified by Cohen *et al* (1973) for high metal concentrations, satisfies this criterion. The predictions of this theory are well known (Granqvist and Hunderi 1978, Berthier 1986). As can be seen in the formulation, the asymmetric expression of the MG theory predicts a unique type of behaviour for the medium at all compositions: either metallic or dielectric according to the matrix nature. This assumption respects the conduction criterion in the renormalization process presented above but consequently the MG theory cannot account for a percolation transition. On the other hand, the MG theory predicts a sharp resonance in the effective dielectric function, corresponding to the vanishing of the denominator of the explicit expression of ε_e. In real systems, this resonance is attributed to the excitation of a collective mode of the conduction electrons at the metallic cluster surface (Clippe *et al* 1976, Stroud 1979, Hui and Stroud 1986). It is worth noting that the very strong dielectric resonance inherent in the MG theory generally does not agree with experimental results.

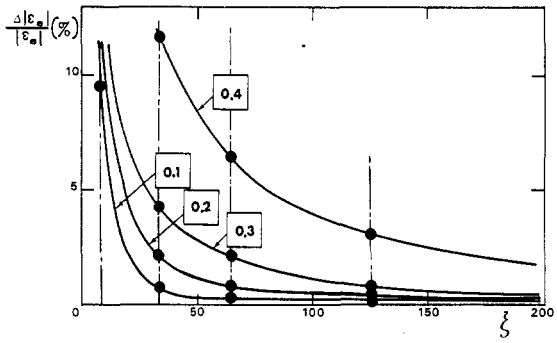

Figure 2. Relative discrepancies between the final value ε_e computed for different initial lattice dimensions ξ, with the $\xi = 512$ lattice result taken as reference. Similar results are obtained above percolation.

Continuing with the renormalization process, we then propose the following transformation:

$$\varepsilon_n = \varepsilon_{n-1}^{ma}(1 + \tfrac{2}{3}q\alpha)/(1 - \tfrac{1}{3}q\alpha) \tag{2}$$

with

$$\alpha = (\varepsilon_{n-1}^{i} - \varepsilon_{n-1}^{ma})/[\varepsilon_{n-1}^{ma} + L_{\parallel}^{i}(\varepsilon_{n-1}^{i} - \varepsilon_{n-1}^{ma})] \tag{3}$$

where ε_{n-1}^{ma} is the dielectric function of the matrix of the block (ε_d or ε_m, following the conduction criterion) at step $n-1$, q the volume fraction of the inclusion (dielectric function ε_{n-1}^{i} and depolarization factor $L_{\parallel}^{i}$) and α its polarizability. ε_n is thus the local effective dielectric function of the block at step n. This computation is repeated for each super-block of the lattice and the whole process is repeated until the effective medium has been reached, when $\xi = 1$ and $\varepsilon_n \to \varepsilon_\infty$. It must be stressed that such a calculation of the local effective dielectric function is an approximation; at any step of the procedure, the dielectric function of the surrounding medium of the four-cell block is assumed to be the effective dielectric function of this block, while it is in fact composed of different other blocks. Nevertheless, this discrepancy between the real and the assumed surrounding medium tends towards zero as the process is converging.

4.1. Percolation threshold

The critical concentration q_c which is a fixed point in the renormalization process can be determined by analysing the gradual change in the concentration of the renormalized lattice (Roussenq *et al* 1976, Reynolds *et al* 1978). Two values of q_c are thus obtained depending on whether sites connected by two corners (along a diagonal) are considered as conducting or not: $q_{c3D} = 0.378 \pm 0.005$ in the conducting case and $q_{c3D} = 0.575 \pm 0.005$ in the non-conducting case.

4.2. Convergence

To determine the convergence of the process, we compare the effective dielectric function computed for different initial lattice dimensions ($\xi = 256$, 128 and 64) with the $\xi = 512$ lattice result taken as a reference (figure 2). The relative difference, as a function

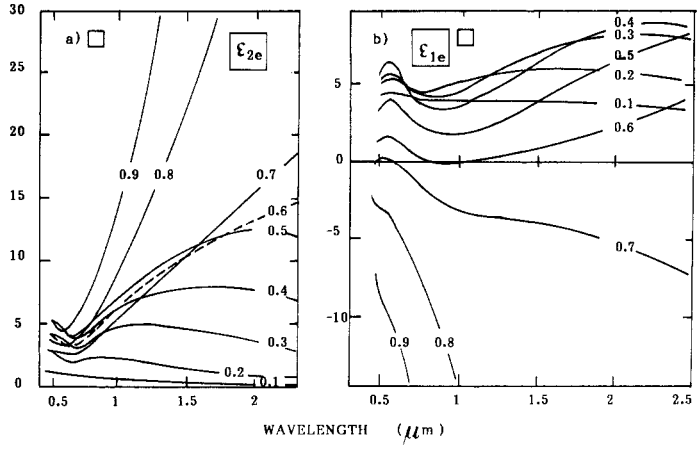

Figure 3. (*a*) Imaginary and (*b*) real parts of the dielectric function of Au–MgO 3D cermet films as calculated by the renormalization process for different Au volume fractions.

of ξ, depends on the concentration q. Far from the percolation threshold, the process rapidly converges. When the concentration and the correlation length increase, the convergence is slower and more iterations are necessary (more than 10), their number tending to infinity at the critical point. In the following, the calculation begins with $\xi = 512$ (nine iterations) at any concentration, which corresponds to the size of the micrograph. This explains the relatively important uncertainties of the results (effective dielectric function and critical exponents).

4.3. Optical properties

The dielectric functions of the initial dielectric and metallic sites correspond, respectively, to MgO ($\varepsilon_1 = 2.6, \varepsilon_2 = 0.05$ = constant) and Au (sum of an interband contribution (Berthier and Lafait 1986) and a Drude contribution: $\varepsilon(\omega) = P - \omega_p^2/\omega(\omega + i/\tau)$ with parameter values $P = 6.5$, $\hbar\omega_p = 9.5$ eV and $\hbar/\tau = 0.6$ eV (a size correction has been introduced by adding a corrective term to the inverse of the relaxation time according to $1/\tau = 1/\tau_0 + v_F/r$, where τ_0 is the bulk relaxation time, r the particle radius and v_F the Fermi velocity; the value of $\hbar/\tau$ corresponds to the average size of the inclusions in the real cermet and is assumed to be a constant whatever the concentration).

An illustration of the results is given in figure 3 where we have plotted the real and imaginary part of the complex effective dielectric function ε_e as a function of the wavelength for various Au concentrations. These calculated curves exhibit the two main characteristic optical features of the cermet films: the gradual crossover between dielectric behaviour ($\varepsilon_{1e} \simeq$ constant > 0, ε_{2e} weak) and metallic behaviour ($\varepsilon_{1e} \ll 0$, $\varepsilon_{2e} \gg 0$) occurs at around $q_c \simeq 0.5$; a dielectric anomaly or surface plasmon resonance is clearly observed in the visible range. These predictions are in qualitative agreement with all the experimental results on random systems (Granqvist and Hunderi 1978, Lamb *et al* 1980) but they are strikingly different from those of the MG theory used at each step of the procedure, or even from those of the mean-field theory (the Bruggeman theory). As can be seen in figure 4, the very strong dielectric resonance inherent in the MG or Bruggeman theories has a weaker amplitude and covers a larger spectral range, in better agreement with the experimental results (Berthier *et al* 1987a). This is due to the

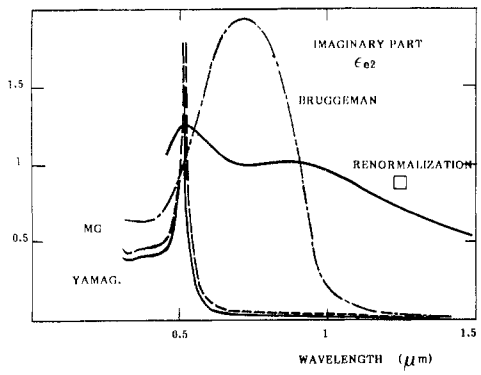

Figure 4. Imaginary part of a Au–MgO granular film as predicted by the MG, Bruggeman and 3D renormalization process 3D theories, and the 2D theory of Yoshida *et al* and Yamaguchi *et al* (YAMAG). $q = 0.2$.

distribution of shapes and orientations of the inclusions which are explicitly taken into account in our model. (We should point out that the generalization of the MG theory to randomly oriented ellipsoids (Granqvist 1978) by averaging the polarizability α over the three principal axes of the ellipsoids does not produce the same effect; it has been shown (Lafait *et al* 1986) that this averaging process corresponds implicitly to the calculation of an effective depolarization factor. In most cases, the excursion of this factor is limited at around $\frac{1}{3}$, i.e. the random by oriented ellipsoids behave like a single sphere for which the MG theory predicts a very strong resonance.)

The other important outcome of our theory is the description of the gradual crossover between the dielectric behaviour and the metallic behaviour around the percolation threshold. We have shown in a previous paper that an analytical expansion of an effective dielectric theory can be given in the framework of the scaling laws, as far as this theory predicts a phase transition (Lafait *et al* 1986). If the metal dielectric function follow the Drude law, where the dielectric resonance vanishes in the infrared, the cermet dielectric function can also be modelled by a Drude function:

$$\varepsilon_e = P_e - \omega_{pe}^2/\omega(\omega + i/\tau_e) \tag{4}$$

where P_e, ω_{pe} and τ_e are effective wavelength-independent parameters. Below the percolation, the effective dielectric function reduces to a constant term $\varepsilon_e = P_e$. The effective polarization P_e can be related to the low-frequency dielectric function, while ω_{pe}^2, which is proportional to the effective number of free carriers, is related to the DC conductivity. These quantities should therefore exhibit a power-law dependence on $|q - q_c|$. A reduced volume fraction q^* can be introduced below and beyond q_c:

$$q^* = \begin{cases} (q - q_c)/q_c \\ (q - q_c)/(1 - q_c) \end{cases} \qquad \text{for} \begin{cases} q < q_c \\ q > q_c \end{cases}.$$

Using this reduced scale, P_e and ω_{pe} have been fitted to the scaling relations $P_e = P_0|q^*|^{-s}$ and $\omega_{pe}^2 = A^2 q^{*t}$ (figure 5). The average values of the exponents of q^* are $s = 0.75 \pm 0.05$ on either side of q_c ($q \gtrless q_c$), and $t = 2.2 \pm 0.1$ for $q > q_c$. These fitted values are independent of the diagonal conditions of conduction. The uncertainties reflect the influences on s and t of variations in the choice of q_c on the one hand and of the small size of the initial lattice for concentrations close to the percolation on the other hand. It is also interesting to note that P_e obeys a power law over a large q^* range (this is confirmed by experimental measurements on 3D systems (Grannan *et al* 1981)) while the power-law

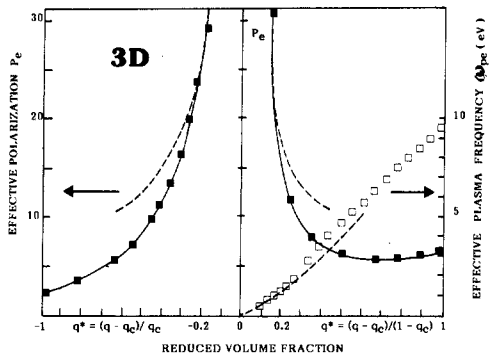

Figure 5. Renormalized effective plasma frequency ω_{pe} and polarization P_e of a free-electron metal–dielectric 3D composite, deduced from a Drude fit of the infrared dielectric function against the reduced filling factor. The broken curves are the best fit to the power-law dependence $P_e = P_0 q^{*-s}$ and $\omega_{pe}^2 = A^2 q^{*t}$.

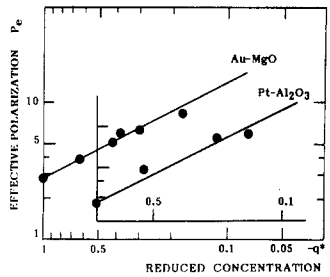

Figure 6. Log–log plot of the experimental effective polarization of Au–MgO and Pt–Al_2O_3 cermet films against the reduced concentration q^*. s(Au–MgO) = 0.71 ± 0.04 and s(Pt–Al_2O_3) = 0.69 ± 0.05.

variation range of the conduction is very limited. The values of s and t which we have found deserve a few comments.

These s and t values are in rather good agreement with the calculations on 3D random systems ($s = 0.73$, $t = 1.94$) (Derrida *et al* 1983) although we used a 2D lattice for the renormalization process. This result is not surprising. According to the random unit-cell concept, by the use of a 3D theory for the calculation of the local effective dielectric function, one implicitly considers a 3D medium with a volume structure identical to that described by the square lattice. A complete 3D renormalization calculation is at present beyond our possibilities and will probably be less instructive as the dimensionality is imposed by the local calculations.

The improvement achieved by our model is well emphasized if one recalls that the MG theory predicts percolation at $q_c = 1$ and that only the mean-field theories predict percolation at $q_c = L = 1$, but always with critical exponents s and t equal to 1, in complete disagreement with the Monte Carlo simulations and the experimental results.

4.4. Application to digital transmission electron micrographs

We shall now apply this model to real systems, namely Pt–Al_2O_3 cermet films. The optical properties of these films have been extensively studied in a previous paper (Berthier *et al* 1987a, b). The morphology of real cermet films is very different from that of a randomly occupied lattice, but experimental measurements confirmed the power-law variation in P_e below percolation. A log–log plot of the real part of the effective dielectric function as a function of q^* is given in figure 6 (for Au–MgO and Pt–Al_2O_3 films). The s exponents deduced from the slope of the two linear variations s(Pt–Al_2O_3) = 0.69 ± 0.05 and s(Au–MgO) = 0.71 ± 0.05 are in good agreement with the numerical results obtained by the renormalization process. This agreement between the model and the experimental results is confirmed by fitting the optical dielectric functions. Figure 7 presents the binarized transmission electron micrographs of two Pt–Al_2O_3 cermet films. In most cases, the concentration on the image is slightly different from the

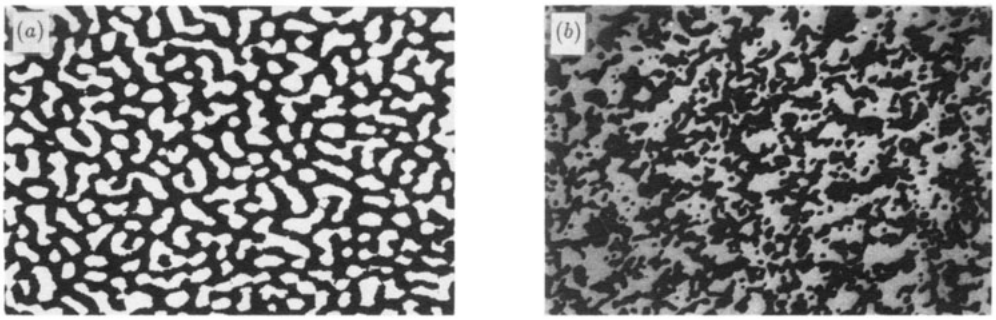

Figure 7. Digitalized transmission electron micrographs of Pt–Al_2O_3 cermet films for Pt volume fractions q of (*a*) 0.42 and (*b*) 0.53.

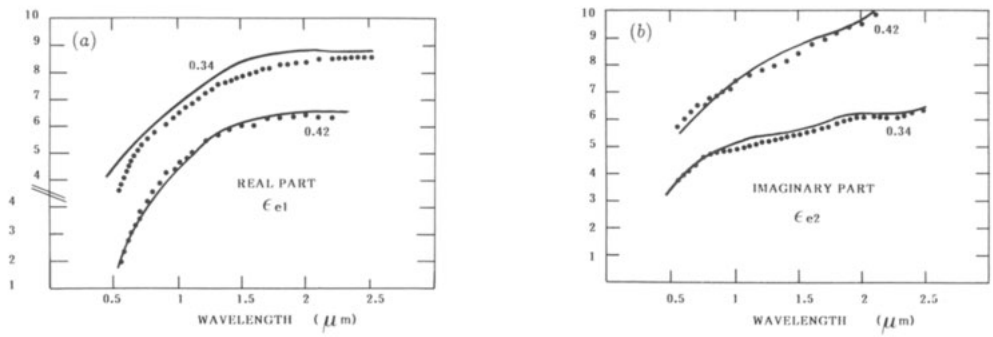

Figure 8. (*a*) Real and (*b*) imaginary parts of the effective dielectric function of Pt–Al_2O_3 thin films (q_{exp} = 0.34 and 0.42) and fits using the renormalization process (q_R = 0.31 and 0.4, respectively).

experimental value. As it can be seen in figures 8 and 9, the spectral variations in the effective dielectric function (figure 8) as well as in the experimental reflection and transmission coefficients (figure 9) are very accurately fitted by the model, even in the vicinity of the percolation threshold.

Although there is no free parameter in the renormalization process, it is possible to attempt a fit by taking the threshold in the binarization process as an adjustable parameter. The concentration of the lattice is modified but the morphology is nearly unchanged. Furthermore, the two diagonal conduction criteria have to be tested. The results generally encompass the experimental values (figure 10).

5. Two-dimensional model

As already pointed out, the recent 2D theory presented by Yoshida *et al* (1971) and Yamaguchi *et al* (1973, 1974) accounts for the substrate effect by the mirror effect expedient. Furthermore, for a given inclusion, the contribution $\boldsymbol{E}''$ to the local field of all the couples dipole–mirror image dipole, assumed to be distributed onto lattice points of a square array, appears explicitly in the formulation and can be neglected if necessary.

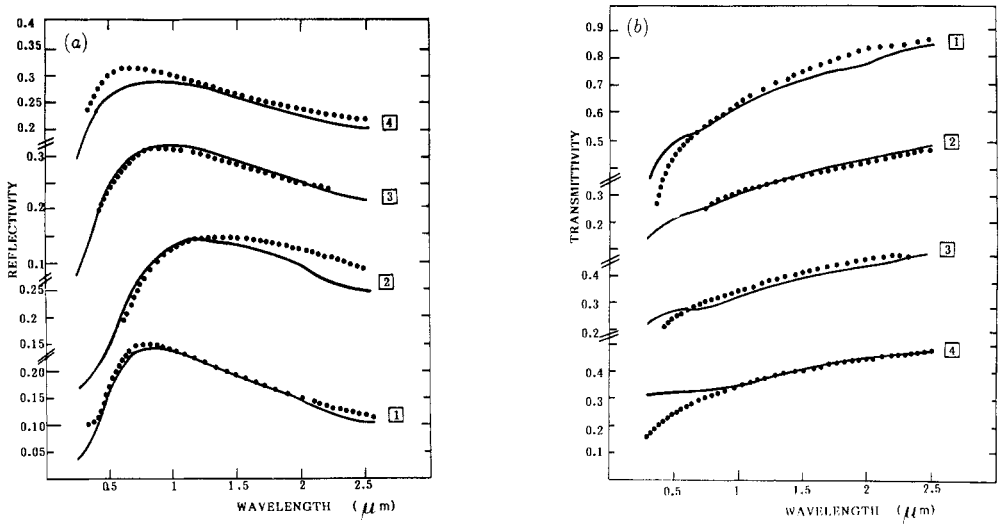

Figure 9. (*a*) Measured reflectivity and (*b*) transmissivity of Pt–Al_2O_3 cermet films and fits using the renormalization process: curves 1, $q = 0.18$; curves 2, $q = 0.34$; curves 3, $q = 0.42$; curves 4, $q = 0.53$.

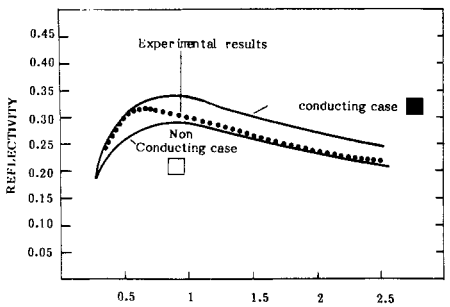

Figure 10. Experimental reflectivity of a Pt–Al_2O_3 cermet film ($q_{exp} = 0.42$) between the renormalization predictions using the two conventions.

By introducing the local field $\boldsymbol{E}_l = \boldsymbol{E}' + \boldsymbol{E}''$ in the classical Clausius–Mossotti equation which expresses the applied electric field as a function of the local field, we obtain for the anisotropic dielectric function of the island film

$$\begin{aligned} \varepsilon_{\parallel}/\varepsilon_a - 1 &= q[1/(F_{\parallel} + g + i\,\Delta g)] \\ 1 - \varepsilon_a/\varepsilon_{\perp} &= q[1/(F_{\perp} + g + i\,\Delta g)] \end{aligned} \tag{5}$$

with

$$\begin{aligned} F_{\parallel} &= L_{\parallel} - (\nu^2/24\eta^3)[(\varepsilon_s - \varepsilon_a)/(\varepsilon_s + \varepsilon_a)] - 0.716[2\varepsilon_a/(\varepsilon_s + \varepsilon_a)](d_w/2a) \\ F_{\perp} &= L_{\perp} - (\nu^2/24\eta^3)[(\varepsilon_s - \varepsilon_a)/(\varepsilon_s + \varepsilon_a)] - 0.716[2\varepsilon_s/(\varepsilon_s + \varepsilon_a)](d_w/a) \end{aligned} \tag{6}$$

and

$$\begin{aligned} g &= \mathrm{Re}[\varepsilon_a/(\varepsilon_i - \varepsilon_a)] \\ \Delta g &= \mathrm{Im}[\varepsilon_a/(\varepsilon_i - \varepsilon_a)]. \end{aligned} \tag{7}$$

L is the classical polarization factor, as defined previously, ε_a is the dielectric function

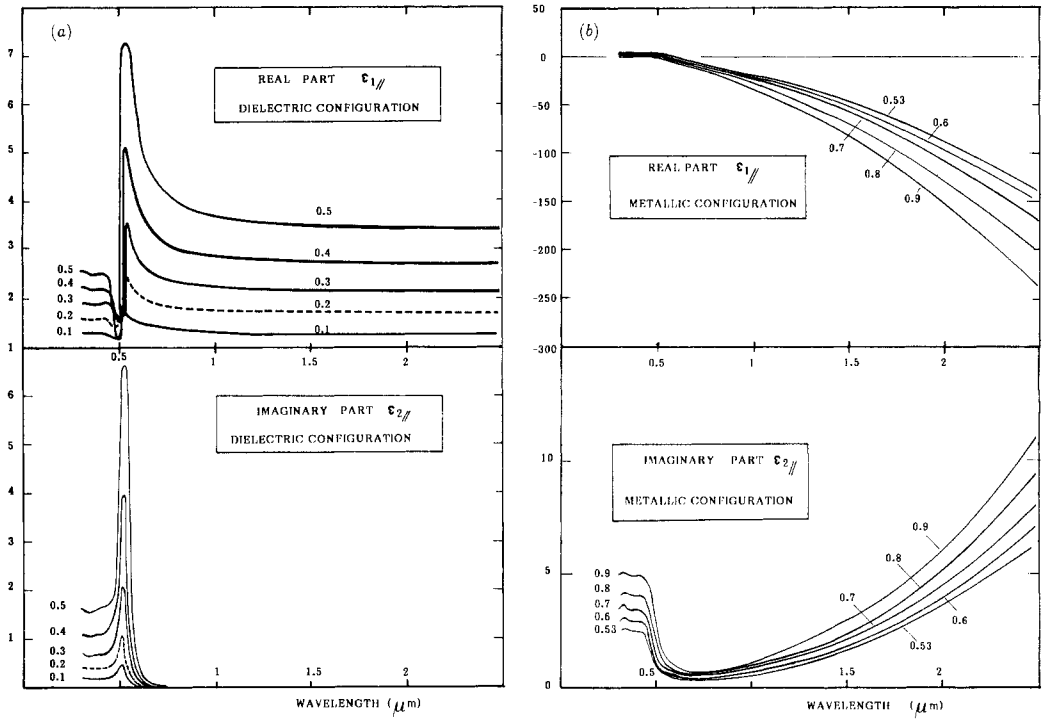

Figure 11. Effective dielectric function of a granular Au film against the wavelength, as calculated by the theory of Yoshida *et al* and Yamaguchi *et al* (component parallel to the surface): (*a*) dielectric matrix; (*b*) metallic matrix. q is the volume concentration of metal.

of the surrounding medium and $\eta = 1/h$. ν is the axial ratio, h is the rotational axis and d_w is the average thickness or the weight thickness.

We first consider the applied field parallel to the substrate for two configurations: a metal in a dielectric; a dielectric in a metal. The variations in $\varepsilon_{\parallel}$ as a function of the wavelength for various concentrations are presented in figure 11. The variations in ε_e as calculated by this approach are similar to those obtained by the MG theory for 3D systems, i.e. a strong dielectric resonance in the visible range shifting towards long wavelengths when the metallic concentration increases and a critical concentration q_c equal to 1. For high metal concentrations the formulation can be inverted in order to model a thin porous metallic film. The crossing from the metal-like to dielectric-like formulation is arbitrary and prohibits a study of the transition in terms of power-law dependences. In this formulation, the interactions are explicitly taken into account. As indicated previously, the interaction term can be neglected in the renormalization process. Equations (5) are unchanged but the last term in the expression for $F_{\parallel}$ or $F_{\perp}$ (equations (6)) is neglected.

5.1. Renormalization process

The local effective dielectric function at step n in a direction parallel or perpendicular to the substrate is given by

$$\varepsilon_n = \varepsilon_{n-1}^{ma} + q\varepsilon_{n-1}^{ma}/[F_{\parallel(\perp)}^{i} + \varepsilon_{n-1}^{ma}/(\varepsilon_{n-1}^{i} - \varepsilon_{n-1}^{ma})] \tag{8}$$

where ε_{n-1}^{ma} and ε_{n-1}^{i} are the effective dielectric functions of the matrix and of the

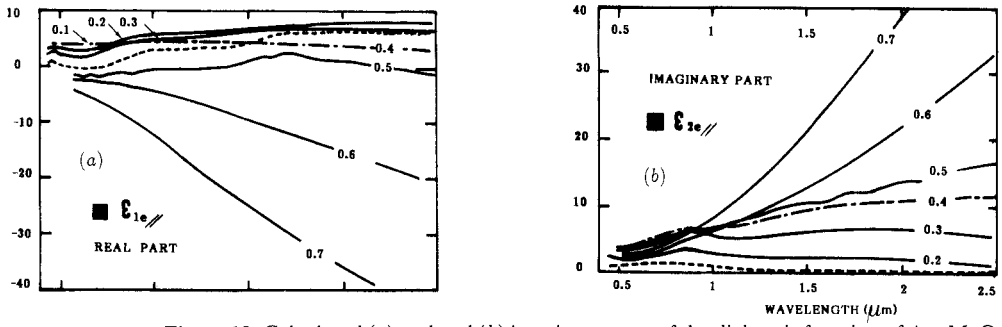

Figure 12. Calculated (*a*) real and (*b*) imaginary parts of the dielectric function of Au–MgO 2D granular films against wavelength for different Au volume fractions q (diagonal conducting case ■).

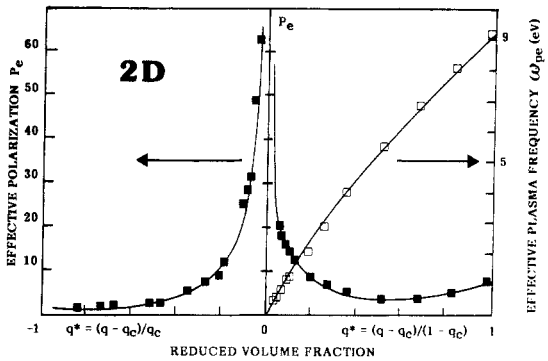

Figure 13. Renormalized effective plasma frequency ω_{pe} and polarization P_e of island films deduced from a Drude fit of the calculated infrared dielectric function against the reduced filling factor.

inclusion of any unit cell at step $n-1$, which are either dielectric or metallic according to the conduction criterion as defined for the 3D model. Following the procedure established for the 3D case, this new model of the optical dielectric function of 2D inhomogeneous media has been tested on a random 512×512 square lattice simulated on a computer. The dielectric functions of the initial dielectric and metallic sites correspond to MgO and Au, with the same values as in the 3D system. The results are presented in figure 12 in the diagonal conducting case for $\varepsilon_{\|}$. The fluctuations observed in the effective dielectric functions for concentrations close to the percolation threshold ($q = 0.4$ and $q = 0.5$) are due to the very slow convergence of the renormalization process in this concentration range. The percolation threshold in these simulated 2D lattices is the same as that determined previously ($q_c = 0.378$ in the conducting case and $q_c = 0.575$ in the non-conducting case). On both sides of these critical concentrations, we have attempted to determine the polarization and conduction critical exponents for the parallel case (figure 13). The calculated values of P_e diverge as $P_e = P_0|q^*|^{-s}$ where P_0 is a constant prefactor very close to ε^{ma}. The average value of s on both sides of q_c is

$$s = 1.35 \pm 0.035 \text{ (for } q < q_c, s = 1.335, \text{ for } q > q_c, s = 1.375).$$

Above percolation, the effective plasma frequency varies as $\omega_{pe}^2 = A^2 q^{*t}$ with $t =$

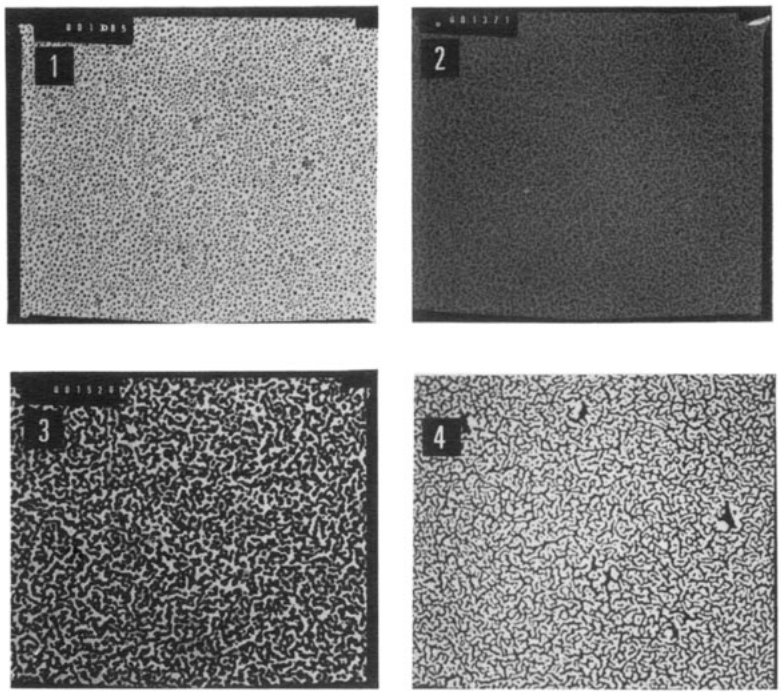

Figure 14. Digitalized transmission electron micrographs of Au island films for Au volume fractions q of 0.27 (micrograph 1), 0.57 (micrograph 2), 0.59 (micrograph 3) and 0.66 (micrograph 4).

1.52 ± 0.25 and $A = 9.35$ eV. The remarks about the uncertainties in s and t, as well as in the validity range of the power laws made in the 3D case, are still valid.

(i) The s- and t-values are independent of the diagonal conduction criterion.

(ii) Our s value is in very good agreement with the calculated value for a 2D random network: $s = 1.35$ (Kirpatrick 1973).

(iii) P_c obeys a power law over a large q^* range, but in contrast with 3D systems there is at present no experimental confirmation of this.

(iv) The plasma frequency follows a power law over a narrow concentration range ($q_c < q < 0.43$) and the t value is slightly different from the theoretical 2D estimates (Clerc *et al* 1983): $t = 1.35 \pm 0.1$. It is obvious that our value has to be improved by applying our model to larger lattices. Nevertheless, the quoted uncertainties include most of the theoretical t values.

5.2. Application to digitized transmission electron micrographs

This model has been applied to real Au granular films, the optical properties of which have been determined by Gadenne (1987). The experimental determination of the effective dielectric function of 2D thin films proves to be rather difficult, especially for the real part, the influence of which on the values of the reflection coefficient R and transmission coefficient T vanishes for concentrations close to the percolation threshold. A more accurate comparison between theoretical and experimental data can be carried out directly on R and T. The calculations have been performed on a set of four Au

Table 1. Characteristics of the four Au granular thin films.

Au granular film	Weight thickness (nm)	Resistivity ($\mu\Omega$ cm)	Au concentration (image treatment)
1	1.42	$>10^8$	0.27
2	2.0	$>10^8$	0.57
3	2.3	368	0.59
4	2.52	177	0.66

granular thin films deposited onto float glass substrates (figure 14), the characteristics of which are presented in table 1.

The critical concentration q_c deduced from the evaluation of the ε_2 against λ slopes in the infrared region is $q_c = 0.58 \pm 0.01$. The morphology of these films is presented in the micrographs in figure 14. These micrographs, after the binarization process, represent the starting point of the renormalization procedure. The calculated effective dielectric functions are presented in figure 15. For comparison with the experimental R and T measurements, the effective thickness of the films has to be known with precision. This is not an easy task because the real morphology of the Au grains in the direction perpendicular to the films cannot be observed. Nevertheless, this effective thickness can be approximated by $E = E_m/q$, where E_m is the mass thickness, supposed to be known with a good precision. In the results presented below, the effective thickness has been introduced as a free parameter.

The calculated optical transmissivity and reflectivity spectra of Au granular films are plotted in figure 16 for four different Au concentrations, close to the percolation threshold. The value of τ used in the calculations is $\hbar/\tau = 0.62$ eV, which corresponds to a particle size of 75 Å.

It can be seen that the present approach reproduces all the characteristic features of the experimental data. There is only quantitative disagreement in the resonance region, especially for the transmission spectra. Better agreement can be obtained by modifying the theoretical film thickness, but the dielectric anomaly is always underestimated. Tentative fits to the absorption band with τ as a free parameter have been carried out.

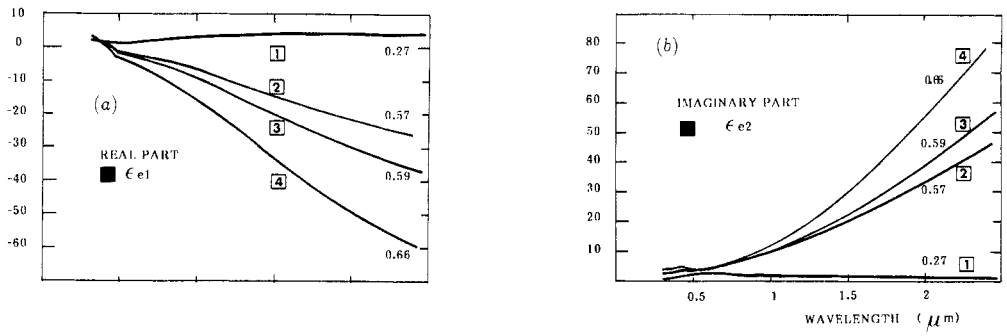

Figure 15. Dielectric function of Au island films by the 2D renormalization process for various Au concentrations.

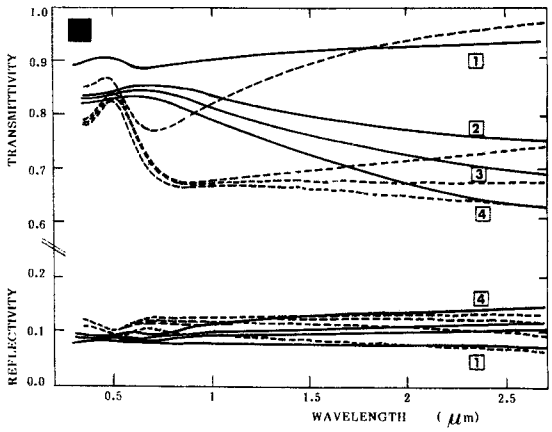

Figure 16. Measured reflectivity and transmissivity of Au island films near the percolation threshold (– – –) compared with the renormalization results (——): curves 1, $q = 0.27$; curves 2, $q = 0.57$; curves 3, $q = 0.59$; curves 4, $q = 0.66$.

The agreement is better but the r values are quite different from the observed diameters of the clusters. On the other hand, it has been noticed that the absorption is well fitted by the renormalization approach if the matrix dielectric function is enhanced ($\varepsilon^{ma} = 2$ instead of 1). The important absorption and dielectric anomaly observed in these materials could then be explained by the presence of very small gold crystallites between the clusters (Gadenne 1976, Gadenne *et al* 1989).

6. Conclusion

We propose a position space renormalization group approach based on the Kadanoff block method, to calculate the effective dielectric function of cermet-type (3D) or island films (2D). These two models use the same rules. The only difference lies in the use of a 2D (Yoshida *et al* and Yamaguchi *et al*) or 3D (MG) effective-dielectric-function theory in the evaluation of the local dielectric function. In both cases, the model predicts the dielectric resonance in the visible range with a fairly correct amplitude and position. The effective dielectric function is found to obey scaling laws with critical exponents $s_{3D} = 0.75$ and $s_{2D} = 1.35$ for the polarization term, and $t_{3D} = 2.2$ and $t_{2D} = 1.52$ for optical conduction. The prediction of the critical exponents s is quite accurate and in good agreement with the experimental and theoretical values. The values of the conduction critical exponents t are slightly larger than theoretical estimates. We believe that this systematic overevaluation is due to the narrow concentration range of validity of the power law and to the very slow convergence of the process in this range. (We are at present limited to 512×512 initial lattices, i.e. to nine successive renormalizations.)

These models have also been applied to digitized transmission electron micrographs of 2D (Au granular films) and 3D (Pt–Al_2O_3 cermet films) systems. In both cases, the agreement of the models with experimental results is confirmed by the fitting of the optical dielectric function or the experimental R and T spectra, even near the percolation threshold. This confirms the essential underlying role of the microstructure in the optical properties of composite systems.

Considering the large number of 3D theories for the effective-dielectric-function calculation, a critical comparison can be carried out with our model. We essentially discuss the predictions of the theories mainly employed: the MG theory (used in our model for the calculation of the local dielectric function of each block) and the

Bruggeman mean-field theory. Comparison with the recent approach of Ping Sheng can be found in the work of Driss-Khodja (1989). It is evident that the MG theory cannot correctly account for the experimental results, because of its fundamental asymmetry. The Bruggeman mean-field theory, which describes a medium where each component exhibits the same shape, seems to be better suited to the structure of our medium, but the fitted values of q (the metallic filling factor) are quite different from the experimental q values and the values of L lead to unrealistic shape parameters.

Considering the formal similarity of the MG theory and the 2D approach of Yoshida *et al* and Yamaguchi *et al*, it is impossible to look for a valuable comparison with our 2D prediction. The renormalization model is—to our knowledge—the only 2D approach predicting an optical crossover. Comparison with few experimental results confirms the self-consistency of this theory.

Our model is the first attempt to introduce the renormalization concept in the effective-dielectric-function calculation, but the actual results look particularly hopeful. We plan a few minor modifications to improve the theory. To remove the ambiguity arising from the 'conducting–non-conducting convention', two different approaches can be explored: a statistical repartition of the conducting and non-conducting blocks, or the use of uneven block lattices ($n = 3$ is the simplest). In particular, for the 2D problem, we also envisage different effective interactions between the neighbouring blocks.

Acknowledgments

We have profited from stimulating discussions with Dr M L Theye and J Lafait. We thank Dr P Gadenne for giving us the 2D Au granular micrographs and characterization.

References

Bedeaux D and Vlieger J 1973 *Physica* **67** 55
—— 1974 *Physica* **73** 287
—— 1983 *Thin Solid Films* **102** 265
Beghdadi A, Constant A, Gadenne P and Lafait J 1984 *Rev. Phys. Appl.* **21** 73
Bernasconi J 1978 *Phys. Rev.* B **18** 2185
Berthier S 1986 *Thèse* Université Pierre et Marie Curie, Paris
—— 1988 *Ann. Phys., Paris* **13** 503
Berthier S and Driss-Khodja K 1989 *Physica* A **157** 357
Berthier S, Driss-Khodja K and Lafait J 1987a *J. Physique* **48** 601
—— 1987b *Europhys. Lett.* **4** 1415
Berthier S and Lafait J 1982 *Thin Solid Films* **89** 213
—— 1986 *J. Physique* **47** 249
Bruggeman D A G 1935 *Ann. Phys., Lpz.* **24** 636
Clerc J P, Giraud G, Roussenq J, Blanc R, Carton J P, Guyon E, Ottavi H and Stauffer D 1983 *Ann. Phys., Paris* **8** 59
Clippe P, Evard R and Lucas A A 1976 *Phys. Rev.* B **14** 1715
Cohen R W, Cody G D, Coutts M D and Abeles B 1973 *Phys. Rev.* B **8** 3689
Derrida B, Stauffer D, Hermann H J and Vanimenus J 1983 *J. Physique Lett.* **44** L701
Driss-Khodja K 1989 *Thèse* Université de Rouen
Gadenne P 1976 *Thèse Troisième Cycle* Université Pierre et Marie Curie, Paris
—— 1987 *Thèse* Université Pierre et Marie Curie, Paris
Gadenne P, Beghdadi A and Lafait J 1988 *Opt. Commun.* **65** 17
Gadenne P, Yagil Y and Deuscher G 1989 *J. Appl. Phys.* **66** 3019

Grannan D M, Garland J C and Tanner D B 1981 *Phys. Rev. Lett.* **46** 375
Granqvist C G 1978 *AIP Conf. Proc.* **40** 196
Granqvist C G and Hunderi O 1978 *Phys. Rev.* B **18** 2897
Hui P M and Stroud D 1986 *Phys. Rev.* B **33** 2163
Kadanoff L P 1966 *Physics* **2** 263
Kadanoff L P, Gotze W, Hamblen D, Hecht R, Lewis E A S, Palciauskas U V, Rayl M, Swift J, Aspnes D and Kane J 1967 *Rev. Mod. Phys.* **39** 395
Kirpatrick S 1973 *Rev. Mod. Phys.* **45** 574
Lafait J, Berthier S and Regalado L E 1986 *SPIE Proc.* **G52** 184
Laibowitz R B, Allesandrini E I and Deutcher G 1982 *Phys. Rev.* B **25** 2965
Lamb W, Wood D and Ashcroft N W 1980 *Phys. Rev.* B **21** 2248
Landau L D and Lifchitz E M 1969 *Electrodynamique des Milieux Continus* (Moscow: Editions de Moscou) p 35
Landauer R 1978 *AIP Conf. Proc.* **40** 2
Maxwell Garnett J C 1904 *Phil. Trans. R. Soc.* **203** 385
—— 1906 *Phil. Trans. R. Soc.* B **205** 237
Mie G 1908 *Ann. Phys., Lpz.* **25** 377
Niklasson G A 1982 *Thèse* Chalmers University, Göteborg
Ping Sheng 1980 *Phys. Rev. Lett.* **45** 60
Reynolds P J, Stanley H E and Klein W 1978 *J. Phys. A: Math. Gen.* **11** L199
Roussenq J, Clerc J P, Giraud G, Ottavi H and Guyon E 1976 *J. Physique Lett.* **37** L99
Stroud D 1979 *Phys. Rev.* B **12** 1783
Wilson K G 1974 *Phys. Rev.* **12** 75
Yagil Y and Deutcher G 1987 *Thin Solid Films* **152** 465
Yamaguchi T, Yoshida S and Kinbara A 1973 *Thin Solid Films* **18** 63
—— 1974 *Thin Solid Films* **21** 173
Yoshida S, Yamaguchi T and Kinbara A 1971 *J. Opt. Soc. Am.* **62** 463